CS Based Wall Ringing and Reverberation Mitigation for Through-the-Wall Radar Imaging

Michael Leigsnering[1], Fauzia Ahmad[2], Moeness G. Amin[2], and Abdelhak M. Zoubir[1]

[1] Signal Processing Group, Institute of Telecommunications
Technische Universität Darmstadt, 64283 Darmstadt, Germany

[2]Radar Imaging Laboratory, Center for Advanced Communications
Villanova University, Villanova, PA 19085 USA

***Abstract*—Wall ringing and reverberation pose a challenging problem for through-the-wall radar image formation algorithms. We propose a novel method based on compressive sensing (CS) that enables high reconstruction quality combined with efficient data collection. A joint wall reverberation and target model is developed and the reconstructed scene is obtained based on a group sparse CS approach. Thus, the wall returns can be separated from the target returns resulting in a clean image. We demonstrate the performance using simulation results.**

I. Introduction

Through-the-wall radar imaging (TWRI) has the potential to image scenes behind walls or other opaque obstacles that cannot be accessed by other means. Various civil and military applications have generated a high interested in this emerging technology [1]–[4].

A major challenge for TWRI are strong reflections from the front wall that distort the received signal. When passing through the front wall, the wave is subject to refractions and reflections from the outer and inner surfaces of the wall. This causes multiple reflections within the wall, leading to what is referred to as wall ringing or reverberation [5]. Wall reverberation, i.e., multiple reflections within the wall, cause wall residuals along the range dimension that may mask targets in the region of interest. Additionally, these multiple reflections cause wall ringing, which creates multiple target copies in the radial direction. The former problem has been tackled by wall mitigation techniques, such as [6], [7]. The latter calls for a multipath exploitation or mitigation scheme [8].

Moreover, highly resolved images require a huge amount of data to be measured, stored and processed. Yoon and Amin [9], first addressed this issue by applying Compressed Sensing (CS) to TWRI, providing good image reconstruction using only a fraction of the full data. CS further proved to be a powerful tool for TWRI, if the scene is sparse or can be sparsely expressed in a convenient basis [9]–[11]. Strong clutter from wall ringing and reverberation, however, results in a densely populated scene.

The work by F. Ahmad was supported by ARO and ARL under contract W911NF-11-1-0536 and the work by M. G. Amin was supported by ONR under grant N00014-11-1-0576.

In this paper, we consider the problem of multiple reflections within the front wall together with a scheme of efficient data collection. It has been shown that wall mitigation on the full data is a viable preprocessing step to obtain a sparse scene [12], [13]. Other methods project the measured data on a space orthogonal to the wall returns [14]. We propose, however, a joint reconstruction approach that captures the wall and target returns simultaneously. By taking wall reverberation and ringing into account, unwanted target copies and wall residuals can be suppressed successfully. The propagation model is a modification of the model proposed by the authors in [15]. We employ a scheme for efficient data collection and a reconstruction approach based on mixed norm regularization. Hence, the wall and targets effects can be separated and a clean image of the scene of interest is obtained. Simulation results are provided to show the effectiveness of the proposed approach.

The remainder of the paper is structured as follows. First, we introduce the signal model for wall and target returns. Based on this, the proposed compressive sensing reconstruction algorithm is described, followed by numerical evaluation and a conclusion.

II. Signal Model

The signal model is formulated using a monostatic stepped-frequency approach [1], [2]. The proposed approach, however, is applicable to other imaging techniques in TWRI.

Assume that the wideband transceivers are placed on a line array consisting of N elements at positions $x_n, n = 0, \ldots, N-1$ at a certain standoff distance from the wall. In the stepped-frequency approach, the wideband pulse is approximated by M monochromatic signals. The frequencies $f_m, m = 0, \ldots, M-1$ are spaced uniformly over the desired bandwidth $f_{M-1} - f_0$.

The received signal, $y[m, n]$, corresponding to the mth frequency and the nth transceiver, can be expressed as the superposition of the target returns $y_{\mathrm{t}}[m, n]$ and the wall

2013 IEEE Radar Conference (RadarCon13)
978-1-4673-5794-4/13/$31.00 ©2013 IEEE

response $y_{\mathrm{w}}[m,n]$,

$$y[m,n] = y_{\mathrm{t}}[m,n] + y_{\mathrm{w}}[m,n]. \tag{1}$$

We divide the region of interest into a regular grid with a finite number of grid points, with N_x and N_y, respectively, representing the points in crossrange and downrange. Let σ_p represent the complex reflectivity corresponding to the pth spatial grid point or the pth target, where $p = 0, 1, \ldots N_x N_y - 1$. Note that absence of a target at a particular grid point is simply represented by a zero value for the corresponding target reflectivity. Therefore, the target return can be expressed as,

$$y_{\mathrm{t}}[m,n] = \sum_{p=0}^{N_x N_y - 1} \sigma_p \exp(-j2\pi f_m \tau_{pn}), \tag{2}$$

where τ_{pn} denotes the round-trip propagation delay between the p-th target and the n-th transceiver. The target reflectivities are assumed constant, independent of frequency and aspect angle. We assume knowledge or accurate estimation of the wall parameters, i.e., the thickness d and the permittivity ε_r. Hence, τ_{pn} can be calculated from geometric considerations [1], [2]. For a method to obtain accurated estimates of the relevant wall parameters, refer to [16].

As walls behave as specular reflectors, the nth transceiver will only receive reflections from the parts of the wall perpendicular to the incident wave [14]. Accordingly, the wall return $y_{\mathrm{w}}[m,n]$ can be expressed as,

$$y_{\mathrm{w}}[m,n] = \sigma_{\mathrm{w}} \exp(-j2\pi f_m \tau_{\mathrm{w}}), \tag{3}$$

where σ_{w} denotes the reflectivity of the wall observed by each antenna element and τ_{w} is the two-way propagation delay from each antenna element to the front wall. As the monostatic array is parallel to the wall, the delay τ_{w} is independent of the transceiver position.

A. Vectorized Measurements

The measurements in (1) can be vectorized for notational convenience. The measured data vector $\boldsymbol{y} \in \mathbb{C}^{MN\times 1}$ is obtained by stacking all MN measurements $y[m,n]$ in one column vector,

$$\boldsymbol{y} = [y[0,0], \ldots, y[M-1,0], \ldots, y[M-1,N-1]]^T. \tag{4}$$

The complex reflectivities σ_p corresponding to targets at positions $\boldsymbol{x}_p$ can be vectorized as,

$$\boldsymbol{s} = [\sigma_0, \sigma_1, \ldots, \sigma_{N_x N_y - 1}]^T. \tag{5}$$

The dictionaries $\boldsymbol{\Phi}_{\mathrm{t}}$ and $\boldsymbol{\phi}_{\mathrm{w}}$ contain the phase terms of the target and wall models, respectively,

$$\begin{aligned} [\boldsymbol{\Phi}_{\mathrm{t}}]_{ip} &= \exp(-j2\pi f_m \tau_{pn}), \qquad m = i \bmod M, n = \lfloor i/M \rfloor, \\ [\boldsymbol{\phi}_{\mathrm{w}}]_i &= \exp(-j2\pi f_m \tau_{\mathrm{w}}), \qquad i = 0, 1, \ldots, MN-1. \end{aligned} \tag{6}$$

Now, using (4 - 6), model (1) can be rewritten as

$$\boldsymbol{y} = \boldsymbol{\Phi}_{\mathrm{t}} \boldsymbol{s}_{\mathrm{t}} + \boldsymbol{\phi}_{\mathrm{w}} \sigma_{\mathrm{w}} \tag{7}$$

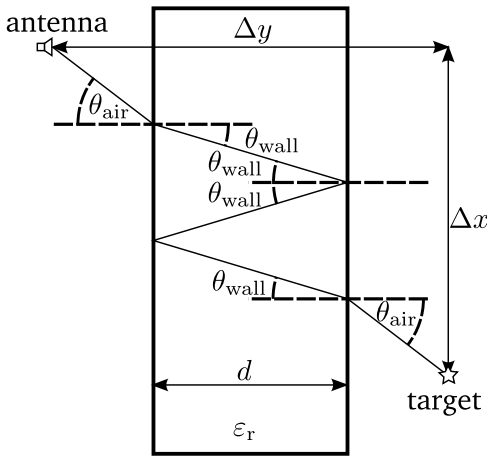

Fig. 1. Wall ringing propagation with $k = 1$ internal bounces

B. Front Wall Multipath

First, we consider the wall ringing contribution on the target return. Subsequently, we turn to the modeling of the wall reverberation. The effect of wall ringing on the target image can be delineated through Fig. 1, which depicts the wall and the incident, reflected, and refracted waves. The distance between the target and the array element in crossrange direction, Δx, can be expressed as

$$\Delta x = (\Delta y - d)\tan\theta_{\mathrm{air}} + d(1+2k)\tan\theta_{\mathrm{wall}}, \tag{8}$$

where Δy is the distance between target and array element in downrange direction, and θ_{air} and θ_{wall} are the angles in the air and in the wall medium, respectively. The integer k denotes the number of internal reflections within the wall. The case $k = 0$ describes the direct path as derived in [1], [2]. From Snell's law,

$$\frac{\sin\theta_{\mathrm{air}}}{\sin\theta_{\mathrm{wall}}} = \sqrt{\varepsilon_{\mathrm{r}}}. \tag{9}$$

Equations (8) and (9) form a nonlinear system of equations that can be solved numerically for the unknown angles, e.g., using the Newton method. Having the solution for the incidence and refraction angles, we can express the one-way propagation delay associated with the wall ringing multipath as [5]

$$\tau(k, \Delta x, \Delta y) = \frac{(\Delta y - d)}{c\cos\theta_{\mathrm{air}}} + \frac{\sqrt{\varepsilon_{\mathrm{r}}} d(1+2k)}{c\cos\theta_{\mathrm{wall}}}, \tag{10}$$

where c is the propagation speed in vacuum.

The wall return including the reverberation can be treated similar to the wall ringing target multipath. Fig. 2 depicts various possible propagation paths which constitute the wall return. The major difference to wall ringing is that the wall reverberation does not involve any interaction with the targets in the scene of interest, see Fig. 2 c). Taking multiple reflections within the front wall into account, we have to change the measurement model (7). We assume a maximum of K different propagation paths that include interactions with the targets and K_{wall} propagation paths that involve only interactions with the front wall. The overall received signal is

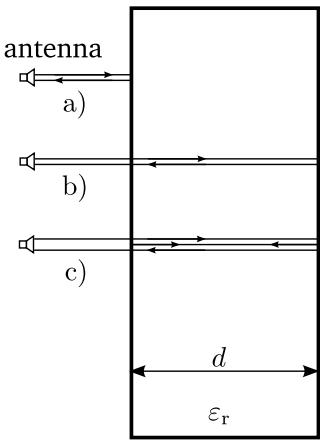

Fig. 2. Various cases of wall reflections: a) reflection from the front face, b) reflection from the back face, c) wall reverberation with multiple internal reflections.

the superposition of all possible propagation paths weighted with the respective amplitudes. Hence, (7) can be modified as

$$\boldsymbol{y} = \boldsymbol{\Phi}_{\mathrm{t}}^{(0)}\boldsymbol{s}_{\mathrm{t}}^{(0)} + \boldsymbol{\Phi}_{\mathrm{t}}^{(1)}\boldsymbol{s}_{\mathrm{t}}^{(1)} + \cdots + \boldsymbol{\Phi}_{\mathrm{t}}^{(K-1)}\boldsymbol{s}_{\mathrm{t}}^{(K-1)} + \boldsymbol{\Phi}_{\mathrm{w}}\boldsymbol{s}_{\mathrm{w}}. \quad (11)$$

The wall ringing contribution is reflected by the summation of several $\boldsymbol{\Phi}_{\mathrm{t}}^{(k)}\boldsymbol{s}_{\mathrm{t}}^{(k)}$ terms, where k corresponds to the number of double-reflections within the front wall, as defined in (8). The wall contribution is similarly defined, where $\boldsymbol{\Phi}_{\mathrm{w}}$ is the concatenation of several phase vectors corresponding to the wall delays $\tau_{\mathrm{w}}^{(k)}$ and $\boldsymbol{s}_{\mathrm{w}} = [\sigma_{\mathrm{w}}^{(0)}, \sigma_{\mathrm{w}}^{(1)}, \ldots, \sigma_{\mathrm{w}}^{(K_{\mathrm{w}}-1)}]^T$ consists of the stacked amplitudes of the wall responses.

Note that, in practice, due to the strong attenuation in wall materials, only two to three wall reverberation responses are typically observed [17].

III. Compressive Sensing and Reconstruction

The ultimate goal of the proposed approach is to obtain a good representation of the scene employing an efficient data acquisition scheme. Hence, we desire a faithful reconstruction using only a fraction of the complete dataset. First, we define how the considered measurements are seleced from the full data. For stepped-frequency operation, as considered in this work, a binary downsampling matrix $\boldsymbol{D} \in \{0,1\}^{J\times MN}$ is a reasonable choice [9], [18]. In this case, one can think of $\boldsymbol{D}$ as an $MN \times MN$ identity matrix, where all but J rows have been deleted. Hence, we obtain an undersampled measurement vector

$$\bar{\boldsymbol{y}} = \boldsymbol{D}\boldsymbol{y}. \quad (12)$$

Applying downsampling operation (12) to the model in (7) yields

$$\bar{\boldsymbol{y}} = \boldsymbol{y} = \boldsymbol{A}_{\mathrm{t}}^{(0)}\boldsymbol{s}_{\mathrm{t}}^{(0)} + \boldsymbol{A}_{\mathrm{t}}^{(1)}\boldsymbol{s}_{\mathrm{t}}^{(1)} + \cdots + \boldsymbol{A}_{\mathrm{t}}^{(K-1)}\boldsymbol{s}_{\mathrm{t}}^{(K-1)} + \boldsymbol{A}_{\mathrm{w}}\boldsymbol{s}_{\mathrm{w}}. \quad (13)$$

where $\boldsymbol{A}^{(r)} = \boldsymbol{D}\boldsymbol{\Phi}^{(r)}, r = 0, 1, \ldots, K-1$ and $\boldsymbol{A}_{\mathrm{w}} = \boldsymbol{D}\boldsymbol{\Phi}_{\mathrm{w}}$.

Using the final measurement equation (13), we propose different schemes for reconstructing the image.

A. Separate Reconstruction

The first and somewhat simplistic approach is to reconstruct the target image regardless of the wall. This is mainly done for comparison so as to demonstrate that more sophisticated reconstruction approaches would provide higher benefits.

For the reconstruction, we assume a model that does not take the wall response into account. However, wall ringing for the target response is considered, hence, the measurements are modeled as

$$\bar{\boldsymbol{y}} = \tilde{\boldsymbol{A}}_{\mathrm{t}}\tilde{\boldsymbol{s}}_{\mathrm{t}}. \quad (14)$$

The vector $\tilde{\boldsymbol{s}}_{\mathrm{t}} \in \mathbb{C}^{N_x N_y K\times 1}$ is obtained by stacking the various vectors of the scene of interest as

$$\tilde{\boldsymbol{s}}_{\mathrm{t}} = \left[\left(\boldsymbol{s}^{(0)}\right)^T \ldots \left(\boldsymbol{s}^{(K-1)}\right)^T\right]^T, \quad (15)$$

and the new measurement matrix $\tilde{\boldsymbol{A}}_{\mathrm{t}} \in \mathbb{C}^{J\times N_x N_y K}$ has the form

$$\tilde{\boldsymbol{A}}_{\mathrm{t}} = [\boldsymbol{A}^{(0)}\ \boldsymbol{A}^{(1)}\ \cdots\ \boldsymbol{A}^{(K-1)}]. \quad (16)$$

Since the sub-images $\boldsymbol{s}^{(k)}$ describe the same underlying scene, the support of these subimages must be equal. Hence, we propose a reconstruction approach based on a group-sparsity constraint that takes the properties of $\tilde{\boldsymbol{s}}_{\mathrm{t}}$ into account. This can be achieved by using ℓ_1 minimization using a mixed $\ell_1 - \ell_2$ norm regularization [19]

$$\hat{\tilde{\boldsymbol{s}}}_{\mathrm{t}} = \arg\min_{\tilde{\boldsymbol{s}}_{\mathrm{t}}} \frac{1}{2}\|\bar{\boldsymbol{y}} - \tilde{\boldsymbol{A}}_{\mathrm{t}}\tilde{\boldsymbol{s}}_{\mathrm{t}}\|_2^2 + \lambda\|\tilde{\boldsymbol{s}}_{\mathrm{t}}\|_{2,1}, \quad (17)$$

where

$$\|\tilde{\boldsymbol{s}}_{\mathrm{t}}\|_{2,1} := \sum_{p=0}^{N_x N_y - 1} \left\| \left[s_p^{(0)}, s_p^{(1)}, \ldots, s_p^{(K-1)}\right]^T \right\|_2, \quad (18)$$

and λ is the so-called regularization parameter. The convex optimization problem (17) can be solved using the freely available toolbox SparSA [19]. A single composite image of the scene is obtained by adding the magnitudes of the reconstructed subimages.

Two remarks about the reconstruction should be noted. First, the choice of the regularization parameter λ is critical as it determines the trade-off between sparsity and fidelity to the measurements. We used a simple heuristic [20] in setting $\lambda = c\|\tilde{\boldsymbol{A}}_{\mathrm{t}}^H\tilde{\boldsymbol{y}}\|_\infty$, where $(\cdot)^H$ denotes the Hermitian transpose and $0 < c < 1$ is a constant. In our simulation, we use $c = 0.15$, which provided good results. More sophisticated methods for choosing the regularization paramater based on cross-validation have been proposed in [18]. Second, in the mixed-norm regularization term (18), different weightings for the returns could be included, as the amplitudes are expected to get weaker and weaker. However, this will not affect the group-sparsity of the vector $\hat{\tilde{\boldsymbol{s}}}_{\mathrm{t}}$. A group of pixels (across the different propagation paths) can either be on or off, which solely determines the sparsity. An additional weighting, hence, has only a minor effect and was omitted in our formulation. The weakening amplitude is captured by smaller pixel values for larger values of k.

B. Joint Group Sparse Reconstruction

As a second approach, we reconstruct the wall and target image jointly considering the full signal model (13) stacking all unknowns into one tall vector,

$$\bar{\boldsymbol{y}} = \boldsymbol{A}_{\mathrm{j}} \boldsymbol{s}_{\mathrm{j}} = [\tilde{\boldsymbol{A}}_{\mathrm{t}} \ \boldsymbol{A}_{\mathrm{w}}] \begin{bmatrix} \tilde{\boldsymbol{s}}_{\mathrm{t}} \\ \boldsymbol{s}_{\mathrm{w}} \end{bmatrix}, \tag{19}$$

From the above high-dimensional joint model of (19), we can pose the reconstruction problem using a modified group sparse regularization term. The convex optimization problem can be expressed as

$$\hat{\boldsymbol{s}}_{\mathrm{j}} = \arg\min_{\boldsymbol{s}_{\mathrm{j}}} \frac{1}{2} \|\bar{\boldsymbol{y}} - \boldsymbol{A}_{\mathrm{j}} \boldsymbol{s}_{\mathrm{j}}\|_2^2 + \lambda \rho_{\mathrm{j}}(\boldsymbol{s}_{\mathrm{j}}). \tag{20}$$

where

$$\rho_{\mathrm{j}}(\boldsymbol{s}_{\mathrm{j}}) := \sum_{p=0}^{N_x N_y - 1} \left\| \left[s_p^{(0)}, s_p^{(1)}, \ldots, s_p^{(K-1)} \right]^T \right\|_2 + \|\boldsymbol{s}_{\mathrm{w}}\|_2 . \tag{21}$$

The difference lies in the choice of the regularizer (21). Our choice stems from the fact that all target sub-images should have a common support and wall reflections are either present or not. This is achieved by grouping the pixels of the target sub-images and the wall reflection coefficients separately. The final output image is again obtained by the summation of the magnitudes.

IV. Results

For the simulation, a 77-element uniform linear monostatic array with an inter-element spacing of 1.9 cm is used for imaging. The origin of the coordinate system is chosen to be at the center of the array. The concrete front wall is located parallel to the array at 2.44 m downrange and has a thickness $d = 20$ cm and relative permittivity $\epsilon = 7.6632$. A stepped-frequency signal, consisting of 801 equally spaced frequency steps covering the 1 to 3 GHz band is employed for scene interrogation. This is a typical frequency range for through-the-wall radar and a reasonable trade-off between down-range resolution and wall attenuation [17].

We simulate two scenarios with two point targets each. In Scenario a, the targets are located at $(0.31, 3.6)$ m and $(-0.62, 5.2)$ m, whereas in Scenario b, the targets are located at $(0.31, 3.6)$ m and $(2.5, 5.9)$ m. Reflections from the front and back faces of the wall as well as one wall reverberation are considered, resulting in a total of three propagation paths for the wall model. The target model accounts for two wall ringing responses in addition to the direct path. White noise with 0 dB SNR is added to the simulated measurements. For comparison, the beamformed images using the full data record are depicted in Figure 3. For the proposed CS reconstructions, we use one-fourth of the array elements and one-fourth of the frequencies. The corresponding results, averaged over 100 Monte Carlo runs, are provided in Figs. 4 and 5. The true postions of the targets are marked with a small circle.

The conventional CS reconstruction results considering only the direct propagation path, i.e., (17) with $K = 1$, are depicted in Figs. 4a and 5a. As the wall reverberations and ringing are not accounted for in this reconstruction model, the wall returns including reverberation and the targets plus their wall ringing copies are all visible. Separate reconstruction of the target scene, without taking the wall response into consideration, was performed with the proposed group sparse CS approach, i.e., (17) with $K = 3$, see Figs. 4b and 5b. This method also does not lead to good results. The wall response is very strong and some spurious targets are introduced in the reconstructed target image. However, if the wall model is properly incorporated in the reconstruction algorithm through (20), the group sparse approach leads to excellent results, refer to Figs. 4c and 5c. The wall response is perfectly suppressed and the two targets are clearly visible.

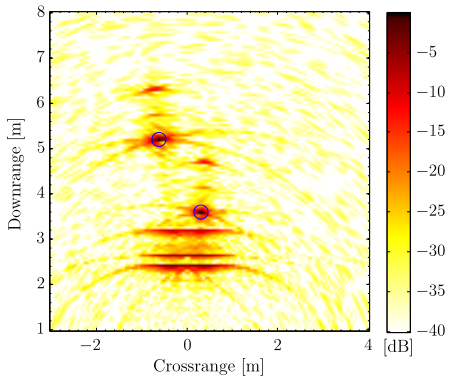

(a) Scenario a

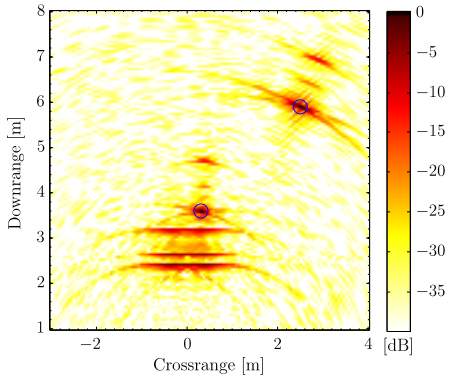

(b) Scenario b

Fig. 3. Conventional DSBF reconstruction using all measurements.

V. Conclusion

A joint wall and target model for TWRI data was introduced. Based on this model, a group sparse reconstruction approach with efficient data collection was developed. Simulation results showed good system performance, featuring a clean image with suppressed wall reverberation and ringing.

References

[1] F. Ahmad and M. Amin, "Multi-location wideband synthetic aperture imaging for urban sensing applications," *Journal of the Franklin Institute*, vol. 345, no. 6, pp. 618 – 639, September 2008.

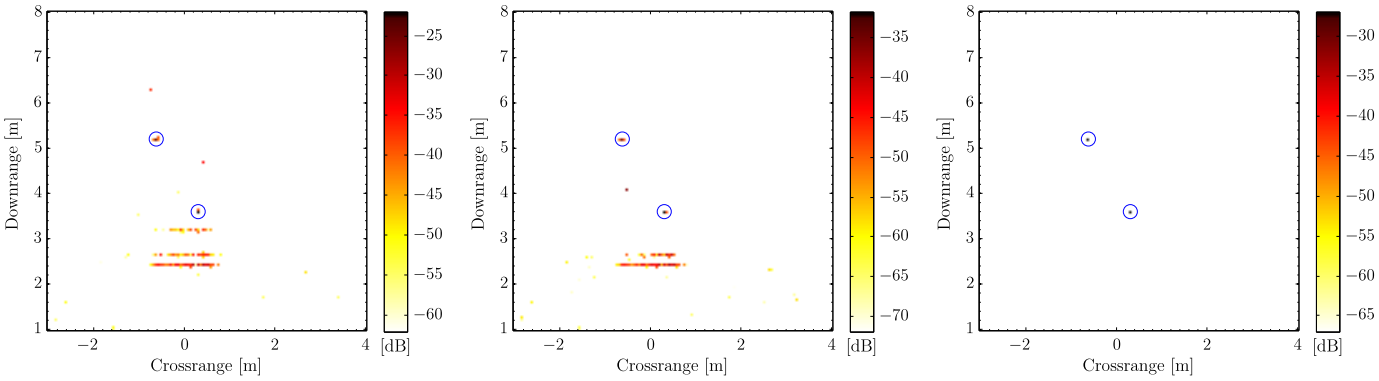

(a) Simple Rec. (b) Separate GS Rec. (c) Joint GS Rec.

Fig. 4. Scenario a: Reconstruction results using one fourth of both the array elements and frequency bins for image formation.

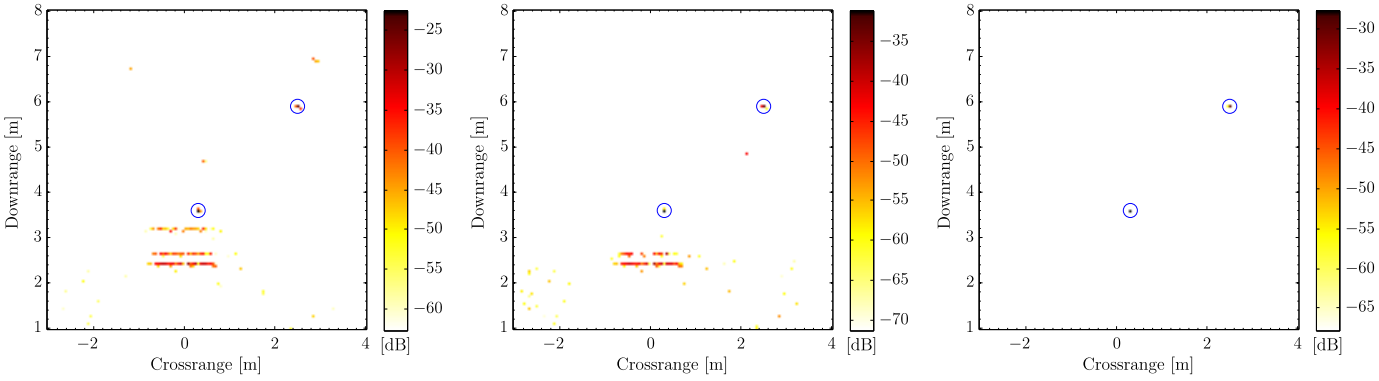

(a) Simple Rec. (b) Separate GS Rec. (c) Joint GS Rec.

Fig. 5. Scenario b: Reconstruction results using one fourth of both the array elements and frequency bins for image formation.

[2] M. Amin and F. Ahmad, "Wideband synthetic aperture beamforming for through-the-wall imaging [lecture notes]," *IEEE Signal Processing Magazine*, vol. 25, no. 4, pp. 110 –113, july 2008.

[3] E. Baranoski, "Through-wall imaging: Historical perspective and future directions," *Journal of the Franklin Institute*, vol. 345, no. 6, pp. 556 – 569, September 2008.

[4] M. Amin, Ed., *Through-the-Wall Radar Imaging*. CRC Press, 2010.

[5] A. Karousos, G. Koutitas, and C. Tzaras, "Transmission and reflection coefficients in time-domain for a dielectric slab for UWB signals," in *IEEE Vehicular Technology Conference*. IEEE, 2008, pp. 455–458.

[6] Y.-S. Yoon and M. Amin, "Spatial filtering for wall-clutter mitigation in through-the-wall radar imaging," *IEEE Transactions on Geoscience and Remote Sensing*, vol. 47, no. 9, pp. 3192 –3208, Sept. 2009.

[7] F. H. C. Tivive, A. Bouzerdoum, and M. G. Amin, "An SVD-based approach for mitigating wall reflections in through-the-wall radar imaging," in *Proc. IEEE Radar Conf. (RADAR)*, 2011, pp. 519–524.

[8] P. Setlur, M. Amin, and F. Ahmad, "Multipath model and exploitation in through-the-wall and urban radar sensing," *IEEE Transactions on Geoscience and Remote Sensing*, vol. 49, no. 10, pp. 4021–4034, 2011.

[9] Y.-S. Yoon and M. Amin, "Compressed sensing technique for high-resolution radar imaging," in *Proceedings of SPIE*, vol. 6968, no. 1, 2008, p. 69681A.

[10] F. Ahmad and M. G. Amin, "Through-the-wall human motion indication using sparsity-driven change detection," *IEEE Transactions on Geoscience and Remote Sensing*, vol. 51, no. 2, pp. 881 –890, feb. 2013.

[11] M. Leigsnering, C. Debes, and A. Zoubir, "Compressive sensing in through-the-wall radar imaging," in *IEEE International Conference on Acoustics, Speech and Signal Processing*, May 2011.

[12] E. L. Targarona, M. G. Amin, F. Ahmad, and M. Nájar, "Wall mitigation techniques for indoor sensing within the cs framework," in *Proc. Seventh IEEE workshop on sensor array and multi-channel signal processing*, 2012.

[13] E. Lagunas, M. G. Amin, F. Ahmad, and M. Najar, "Joint wall mitigation and compressive sensing for indoor image reconstruction," *IEEE Transactions on Geoscience and Remote Sensing*, vol. 51, no. 2, pp. 891 –906, feb. 2013.

[14] F. Ahmad and M. Amin, "Partially sparse reconstruction of behind-the-wall scenes," in *Proc. SPIE Symposium on Defense, Security, and Sensing, Compressive Sensing Conference*, vol. 8365, April 2012.

[15] M. Leigsnering, A. Zoubir, F. Ahmad, and M. Amin, "Multipath exploitation in through-the-wall radar imaging using sparse reconstruction," *IEEE Transactions on Aerospace and Electronic Systems*, 2012, submitted for publication.

[16] C. Thajudeen, A. Hoorfar, and W. Zhang, "Estimation of frequency-dependent parameters of unknown walls for enhanced through-the-wall imaging," in *IEEE International Symposium on Antennas and Propagation (APSURSI)*, july 2011, pp. 3070 –3073.

[17] C. Thajudeen, A. Hoorfar, F. Ahmad, and T. Dogaru, "Measured complex permittivity of walls with different hydration levels and the effect on power estimation of twri target returns," *Progress in Electromagnetic Research B*, vol. 30, pp. 177–199, 2011.

[18] A. Gurbuz, J. McClellan, and W. Scott, "A compressive sensing data acquisition and imaging method for stepped frequency GPRs," *IEEE Transactions on Signal Processing*, vol. 57, no. 7, pp. 2640 –2650, July 2009.

[19] S. Wright, R. Nowak, and M. Figueiredo, "Sparse reconstruction by separable approximation," *IEEE Transactions on Signal Processing*, vol. 57, no. 7, pp. 2479–2493, 2009.

[20] S.-J. Kim, K. Koh, M. Lustig, S. Boyd, and D. Gorinevsky, "An interior-point method for large-scale l1-regularized least squares," *IEEE Journal of Selected Topics in Signal Processing*, vol. 1, no. 4, pp. 606–617, 2007.